



## Late Paleoproterozoic bimodal magmatic rocks in the Nimchak Granite Pluton of the Bathani volcano-sedimentary sequence, Eastern India: implications for the Columbia supercontinent formation with respect to the Indian landmass

Bibhuti Gogoi <sup>1,\*</sup>

<sup>1</sup> Department of Geology, Cotton University, Guwahati, Assam, India- 781001

### ARTICLE INFO

Submitted: August 2020

Accepted: January 2022

Available on line: January 2022

\* Corresponding author:  
bibhuti.gogoi.baruah@gmail.com

Doi: 10.13133/2239-1002/16978

How to cite this article:  
Gogoi B. (2022)  
Period. Mineral. 91, 1-20

### ABSTRACT

The Nimchak Granite Pluton occurs within the Bathani volcano-sedimentary sequence (BVSs) that was punctured by several mafic/dolerite dykes during its evolution. The BVSs is positioned in the northernmost part of the Chotanagpur Granite Gneiss Complex (CGGC) of Central Indian Tectonic Zone, Eastern India. Two mafic dykes are preserved in the pluton that were emplaced after the entire felsic magma chamber had solidified. The present work discusses geochemical signatures of mafic rocks from the two well-preserved dolerite dykes and felsic rocks from the host pluton. The mafic and felsic rocks display high LILE/HFSE and LREE/HREE ratios, which are distinctive features of magmas generated in subduction zones. Tectonic discrimination diagrams clearly suggest that the mafic-felsic rocks were generated in a subduction zone tectonic setting with the mafic rocks clearly plotting in the region of 'back-arc basin basalt'. The felsic rocks of the Nimchak Pluton give Th-U-Pb monazite chemical age of 1768 Ma for their emplacement. This particular magmatic event is correlatable to the global phenomenon of the Columbia supercontinent formation. Results presented in this work suggest that the CGGC represents an island arc setting in which the Dalma Volcanic Belt (DVB) constitutes the volcanic arc, while the BVSs constitutes the back-arc rift. The DVB is an arcuate belt of volcanic rocks occupying the central portion of the North Singhbhum Mobile Belt, which occurs to the south of the CGGC. Northward subduction of the southern Singhbhum block underneath the northern Bundelkhand block during the Proterozoic produced the island arc system. The crustal plates involved in this subduction were oceanic plates that were attached to the Singhbhum and Bundelkhand cratons.

Keywords: Central Indian Tectonic Zone; Singhbhum Craton; Bundelkhand Craton; Dalma Volcanic Belt; Nimchak Granite Pluton; island arc system.

### INTRODUCTION

The Central Indian Tectonic Zone is an ENE-WSW trending Proterozoic mobile belt that splits the Greater Indian Landmass into northern and southern crustal provinces. The northern crustal province is composed of the Archaean Bundelkhand Craton as its kernel, while the southern province is an amalgamation of the Dharwar, the

Bastar and the Singhbhum Archaean Cratons (Acharyya, 2003). The northern region of the Central Indian Tectonic Zone is occupied by the Mahakoshal Mobile Belt, which is a narrow rift zone confined between the Moho-reaching Son-Narmada lineaments. The wider southern domain of the Central Indian Tectonic Zone is constituted by the Sausar Mobile Belt, the composite Chotanagpur Granite

Gneiss Complex-North Singhbhum Mobile Belt and the Shillong Plateau Gneissic Complex.

The Chotanagpur Granite Gneiss Complex (CGGC) occupies the central domain of the Central Indian Tectonic Zone. To the east of this central domain lies the Shillong Plateau Gneissic Complex and to the west lies the Sausar Mobile Belt. The Bathani volcano-sedimentary sequence (BVSs) lies to the north of the central domain and the North Singhbhum Mobile Belt lies to its south. The BVSs is now considered as the eastern continuation of the Mahakoshal belt (Saikia et al., 2014, 2017, 2019; Gogoi et al., 2020). The sandwiched portion between these two mobile belts, i.e. the BVSs and the North Singhbhum Mobile Belt, is dominated by gneisses, migmatites and massive granites. One of the most conspicuous features occupying the central portion of the North Singhbhum Mobile Belt is the arcuate-shaped Dalma Volcanic Belt (DVB). The DVB evolved concomitantly with the CGGC and is tectonomagmatically related to the latter (Acharyya, 2003). To the south of the North Singhbhum Mobile Belt lies the Archaean Singhbhum Craton.

A number of geotectonic models have been suggested to explain the origin and evolution of the CGGC. The models include (a) northward convergence of an ancient oceanic slab attached to the Singhbhum Craton beneath CGGC microcontinent. Continued subduction resulted in collision and annexation of the Singhbhum Craton with the CGGC (Sarkar and Saha, 1977; Sarkar, 1982; Mahato et al., 2008); (b) southward convergence of the northern crustal block underneath the southern crustal block with continental collision at ca. 1600-1500 Ma was proposed by Acharyya (2003); (c) plume-driven rifting between the Chotanagpur Complex and the Singhbhum Craton that led to the formation of an ensialic basin. The rift basin is represented by the North Singhbhum Mobile Belt. The development of the rift basin was followed by mafic magmatism and shortening of the crust (Mukhopadhyay, 1990; Gupta and Basu, 2000); (d) a tectonothermal model involving two stages of accretion at ca. 1560 Ma and 1000 Ma was proposed for the evolution of the composite North Singhbhum Mobile Belt and CGGC by Rekha et al. (2011). The existence of such diversified hypotheses implies that the origin and evolution of the CGGC is still contentious.

In the present work geochemical signatures of the felsic and mafic rocks from the Nimchak Granite Pluton (NGP) of the BVSs are discussed. The mafic rocks are preserved as intrusive dolerite dykes within the granitic rocks of the NGP. Geochemical results presented in this work suggest that the BVSs represents a back-arc rift basin that evolved contemporaneously with the DVB. The occurrence of two sub-parallel contemporaneous volcanic belts in the northern and southern CGGC offers a unique opportunity

to understand the geotectonic framework of the CGGC during the Proterozoic.

## REGIONAL GEOLOGICAL SETTING

The Central Indian Tectonic Zone is a ca. 1,500 km long Proterozoic mobile belt that divides the Indian subcontinent into the Northern Indian Block and the Southern Indian Block. The northern block is composed of the Bundelkhand Craton as its kernel, while the southern block is an association of Singhbhum, Bastar and Dharwar Cratons (Figure 1a). The Central Indian Tectonic Zone may be broadly categorized into three tectonic blocks from west to east, which include the western Sausar Mobile Belt, the central CGGC and the eastern Shillong Plateau Gneissic Complex (Acharyya, 2003).

The CGGC is a ca. 80,000 km<sup>2</sup> high-grade terrain comprising granite gneisses, migmatites, metasedimentary enclaves, granulites, leptynite and khondalite, which have been intruded by granite, mafic and ultramafic rocks, anorthosite, syenite, pegmatite and aplite (Mukherjee and Ghose 1992; Mahadevan 2002). This high-grade terrain is sandwiched between the BVSs and the North Singhbhum Mobile Belt to the north and south, respectively.

The North Singhbhum Mobile Belt is a ca. 200 km long and 50 km wide arcuate deformed belt, which separates the deformed rocks of the CGGC and the Archaean Singhbhum Craton. It comprises mainly greenschist to amphibolite grade phyllites and schists skirting the centrally-positioned DVB. The DVB is an arcuate-shaped metavolcanic suite of about 200 km in length and 2.5 km in thickness within the Singhbhum Mobile Belt (Figure 1b). This metavolcanic suite of rocks characterizes explosive volcanism as indicated by the presence of sub-aerial basaltic flows along with agglomerate and tuffaceous rocks. In general, the Dalma volcanic rocks may be classified into four distinct lithological units (Alvi et al., 2019): (a) altered ultramafic rocks (b) metagabbro and metadolerite (c) fragmental mafic rocks consisting of agglomerate and breccia (d) non-fragmental mafic rocks. An island arc tectonic setting has been proposed for the Dalma volcanics (Naha and Ghosh, 1960; Alvi et al., 2019, Chakraborty et al., 2019) that evolved during the Late Palaeoproterozoic time (Chatterjee et al., 2013; Bhattacharya et al., 2015).

The northern periphery of the CGGC is demarcated by the BVSs, which is a narrow rift basin bounded by two Moho-reaching lineaments (Figure 1 b,c). The volcano-sedimentary litho assemblage is well exposed over an estimated aerial distance of 40 km with the type locality situated near Bathani village in the Indian state of Bihar. The dominant rock types encountered in the type locality include pillow and massive basalts, rhyolite, mafic pyroclasts, phyllitic tuff, quartzite, phyllite, chert and

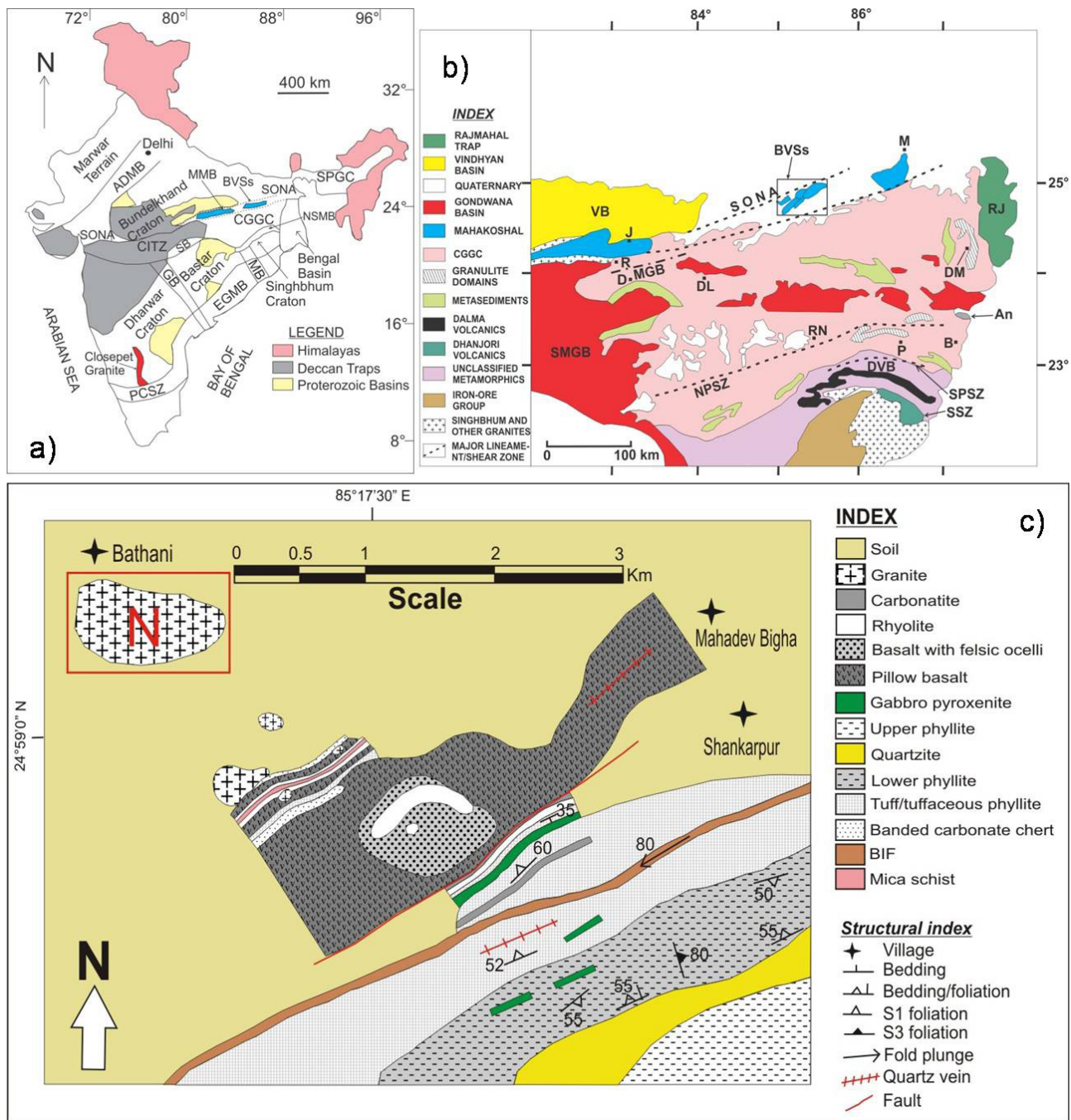


Figure 1. a) Geological map of India displaying the location of Central Indian Tectonic Zone (CITZ). The Bathani Volcano Sedimentary sequence (BVSS) lies in the northern fringe of the Chotanagpur Granite Gneiss Complex (CGGC) within the Son-Narmada (SONA) lineaments. (modified after Pradhan et al., 2009). ADMB - Aravalli Delhi Mobile Belt, EGMB - Eastern Ghats Mobile Belt, GB - Godvari Basin, MB - Mahanadi Basin, PCSZ - Palghat-Cauvery Shear Zone, SG - Southern Granulites, SPGC - Shillong Plateau Gneissic Complex. b) Geological map of CGGC (modified after Acharyya, 2003). An - Anorthosite, B - Bankura, BVSS - Bathani volcano-sedimentary sequence, D - Dudhi, DL - Daltonganj, DM - Dumka, DVB - Dalma Volcanic Belt, J - Jirgadandi, M - Munger, MGB - Makrohar Granulite belt, NPSZ - North Purulia Shear Zone, PR - Purulia, R - Rihand - Renuagar Area, RJ - Rajmahal Hills, RN - Ranchi, SMGB - Son Mahanadi Gondwana Basins, SONA - Son Narmada Lineament, SPSZ- South Purulia Shear Zone, SSZ - Singhbhum Shear Zone, VB - Vindhyan Basin. c) Geological map of BVSS displaying the location of Nimchak Pluton denoted by 'N' (modified after Ahmad and Paul, 2013).

banded iron. A single litho-unit of garnet-mica schist is also found to be in contact with mafic pyroclastic rock and chert. The volcano-sedimentary litho-assemblage has been intruded by granitic bodies, which occur as dome-like structures or hillocks. In general, the litho-units of the BVSs can be categorized into three broad units (Ahmad and Wanjari, 2009): (a) mafic volcanics consisting of pillow basalt, massive basalt and mafic pyroclasts (b) acid volcanics consisting of rhyolite (c) volcano-sedimentary sequence consisting of tuffaceous rocks, quartzite, phyllite, chert and banded iron.

#### GEOLOGY OF THE NIMCHAK GRANITE PLUTON

The NGP is a ca. 1 km<sup>2</sup> felsic magmatic pluton that occurs within the BVSs. The pluton is situated at Nimchak village near Bathani. Two types of granitoids are encountered within the pluton- one coarse grained and the other fine grained. The lower portion of the Nimchak Pluton is dominated by the coarser variety of granite, whereas the upper portion is constituted by the finer variety (Figure 2a). The occurrence of these two varieties of granite suggests that the NGP was a vertically stratified felsic reservoir in which fractional crystallization should have caused the textural variability (Gogoi et al., 2018).

Field observations suggest that the granite pluton was intruded by at least eight mafic/dolerite dykes during the entire crystallization/solidification period of the felsic reservoir. Out of the eight dykes, six dykes interacted with the felsic host indicating magma mixing (Gogoi et al., 2017; Gogoi et al., 2018; Gogoi et al., 2020). These six mafic dykes are traceable in the lower coarse-grained granite. Mafic magmatic enclaves related to these dykes are distributed around them in the host granite. However, the six dykes are untraceable in the upper fine-grained variety owing to the fact that these dykes disintegrated into smaller mafic magmatic enclaves in the upper portion of the Nimchak Pluton. A detailed description about the nature of interaction between the mafic dykes and host granite can be found in Gogoi et al. (2018).

The remaining two dykes share sharp contact with the granitic host (Figure 2b) and cross-cut the entire felsic pluton unlike the other dykes (Figure 2 c,d), which are traceable only in the lower coarse-grained granite. Such field relationships indicate that the two continuous dolerite dykes punctured the Nimchak Pluton after total solidification of the felsic reservoir such that the mafic magma could not interact with the felsic host. On the other hand, the six mafic dykes intruded the felsic pluton when it was in magmatic state that led to the mixing of mafic and felsic magmas. Thus, on the basis of field observations it can be established that the two continuous dolerite dykes are late-stage mafic dykes that intruded the Nimchak Pluton after the intrusion of the six mafic dykes.

Several smaller mafic dykes are seen bifurcating from the two late-stage dykes into the granitic host (Figure 2 e,f). Moreover, since the two dolerite dykes did not interact with the host granite, they are best representative of the parental mafic magmas associated with the BVSs.

#### PETROGRAPHY

Petrographic observations for the present study is restricted to the mafic and felsic rocks of NGP, which include dolerite from the late-stage dykes and granitic rocks that are situated away from the mafic intrusions.

##### Dolerite

For petrographic study, mafic rocks were sampled from the center of the dolerite dykes. The samples show primary magmatic textures suggesting that these rocks have not been affected by any deformational event. Dolerite samples collected from the core show major mineral assemblage of clinopyroxene and plagioclase, while Ti-Fe oxide, amphibole and biotite constitute the minor phases. Laths of plagioclase are observed to be enveloped by clinopyroxene depicting ophitic relationship (Figure 3a). Few clinopyroxene grains show low-degree of alteration to amphibole as indicated by reaction rim at the boundary (Figure 3b).

##### Granite

The granitic rocks display fine-to-coarse grained texture and dominantly consist of quartz, plagioclase, K-feldspar and biotite (Figure 3c). The minor mineral phases include chlorite, muscovite, apatite, epidote, zircon, monazite, titanite and iron-oxide. The mineral grains in this rock mostly range from anhedral to subhedral in shape and generally display allotriomorphic texture. Strain effect is visible in this rock as indicated by fractured grains and wavy extinction in quartz. Kinking is observed in some biotite grains indicating accumulation of high strain. Plagioclase exsolution lamellae within K-feldspar depicting perthitic intergrowth is a common feature in this rock (Figure 3d). Intergrowth of quartz is observed in plagioclase representing myrmekitic texture. Sieve-textured feldspars are a common feature in some of the granitic samples. The presence of both biotite and muscovite suggests that the felsic rocks of the Nimchak Pluton are two-mica granites.

#### ANALYTICAL METHODS

Major oxides and trace elements were analysed using XRF (Bruker S8 Tiger Sequential X-ray Spectrometer with Rh excitation source) following the procedure of Saini et al. (1998, 2000) and rare earth elements (REE) were analysed using ICP- MS (PerkinElmer made SCIEX quadrapole type ICP-MS, ELAN DRC-e), at the Wadia

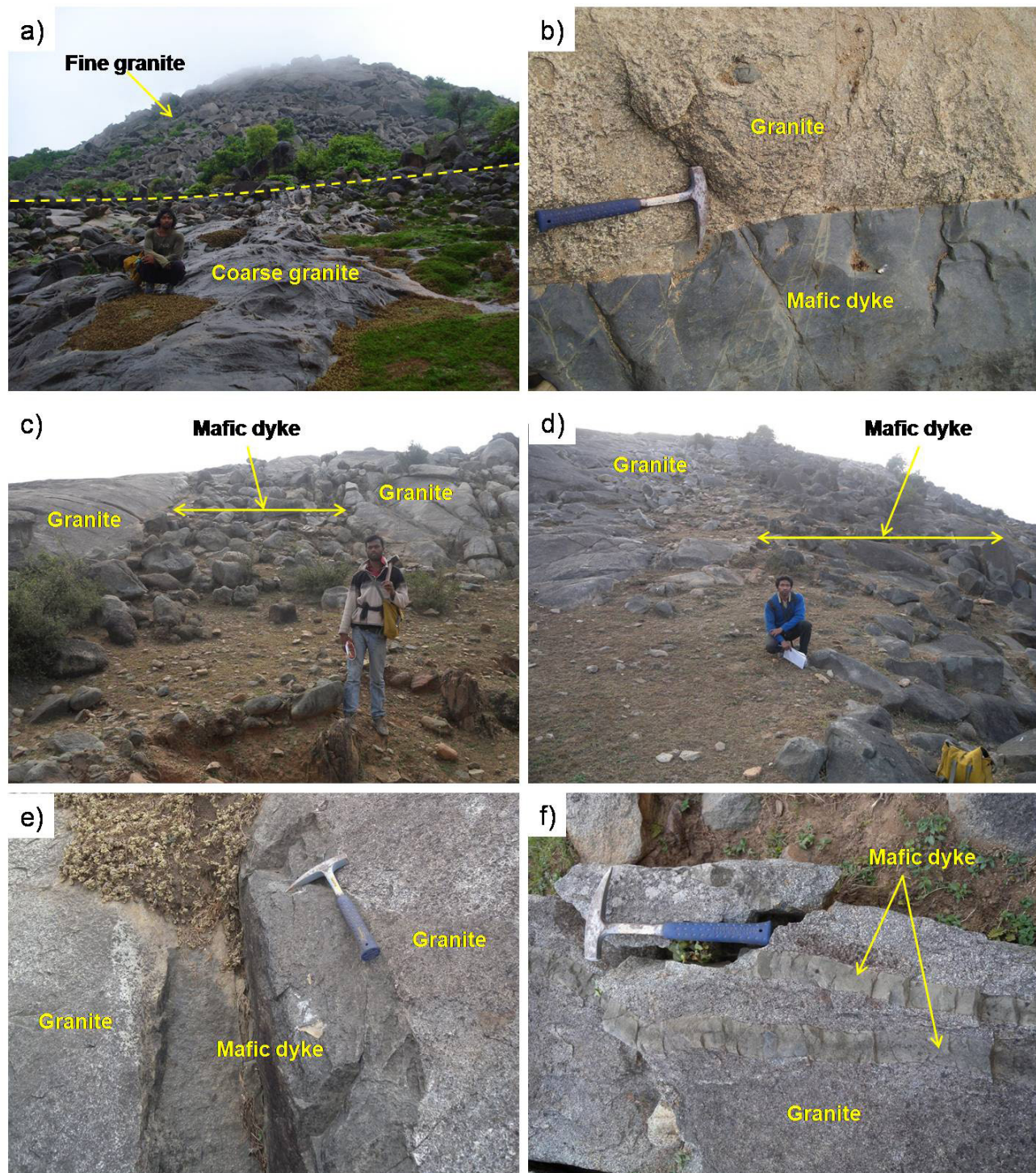


Figure 2. Field photographs displaying a) Contact between the two varieties of granite. The upper granite is fine-grained, while the lower unit is coarse-grained. b) Sharp contact between the late-stage mafic dyke and granitic host. c,d) Late-stage mafic dykes sharing sharp contact with the granitic rocks. e,f) Smaller mafic dykes bifurcating from the two late-stage dykes into the host granitoid.

Institute of Himalayan Geology, Dehradun (India).  
Operating conditions for the major oxides were: No filter,  
Vacuum path, 20/40kV; for trace elements: No filter,

Vacuum path, 55/60kV. The overall accuracy in relative  
standard deviation percentage is <5% for major and minor  
oxides and <12% for the trace elements. The average

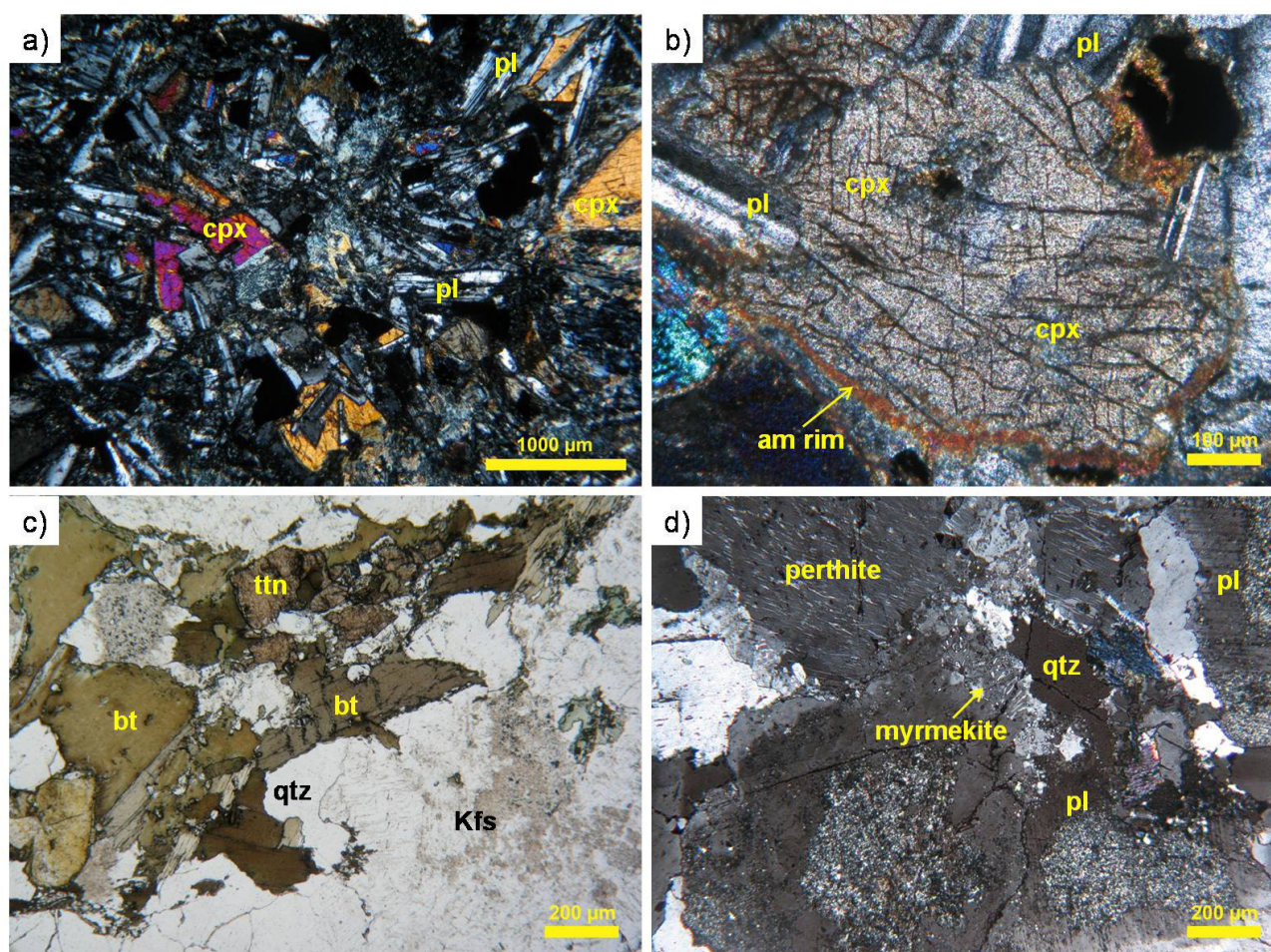


Figure 3. Photomicrographs displaying a) Plagioclase in ophitic relationship with clinopyroxene in the dolerite. b) Clinopyroxene altering to amphibole at the boundary as indicated by the presence of thin reaction rim. c) PPL view of the granite. d) Textural features like perthite and myrmekite observed in the granite. Mineral abbreviations: bt - biotite, cpx - clinopyroxene, Kfs - K-feldspar, pl - plagioclase, qtz - quartz, ttn - titanite.

precision is better than 2.0% (Saini et al., 2007; Purohit et al., 2006). Sample solutions were introduced for rare earth element analysis into the argon plasma using a peristaltic pump and a cross flow nebulizer. The procedures adopted for sample digestion and preparation of solutions were that of Balaram et al. (1990). USGS (BHVO-1, AGV-1) and JGS (JG-2, RGM-1) samples were used as rock standards to minimize matrix effect. RSD for most of the samples is better than 10%.

Chemical dating of monazite was performed using a CAMECA SX 100 electron microprobe at Electron Microprobe Analyzer Laboratory, Geological Survey of India, Faridabad (India). The data were obtained using an acceleration voltage of 20 kV and a beam current of 20 nA. Large polyethylene terephthalate was used for measuring Pb M with a peak counting time of 300 seconds. In order to prevent interference with the Th

$M\alpha$  line, U  $M\alpha$  line was used for uranium with a peak counting time of 200 seconds. The peak counting time for Th  $M\alpha$  was also 200 seconds. A positron emission tomography (PET) crystal was used for measuring both U and Th. Standards used for measuring U, Th and Pb were  $UO_2$ ,  $ThO_2$  and PbS respectively. Meanwhile, standard used to measure La, Ce, Nd, Pr, Sm, Ho, Dy and Gd consisted of a synthetic silica-aluminium glass with 4% rare earth elements. The structural formulae and total concentration of monazite were checked by analyzing 15 elements (Si, P, La, Ce, Pr, Nd, Sm, Gd, Dy, Y, U, Th, Pb, Ca and K). The formulation of Montel et al. (1996) was applied for individual spot ages, while the age probability plot and unmixing of ages were determined using the software Isoplot3 (v.3.71.09.06.19nx; Ludwig, 2001). Unreliability in individual analyses and in the weighted mean ages is quoted at 95% confidence level.

More details about the analytical procedure can be found in Dora et al. (2019).

## GEOCHEMISTRY

### Major oxides

The representative analysis of major oxides is listed in Table 1. The studied rocks may be categorized into two major components; felsic rocks with high  $\text{SiO}_2$  and alkali contents and mafic rocks with low  $\text{SiO}_2$  content. In the  $\text{Na}_2\text{O}+\text{K}_2\text{O}$  vs.  $\text{SiO}_2$  diagram (Middlemost, 1994), the mafic rocks cluster in the gabbro field, while the felsic rocks cluster in the fields of granite, granodiorite, quartz monzonite and diorite (Figure 4a). In the  $(\text{Na}_2\text{O}+\text{K}_2\text{O})-\text{Fe}_2\text{O}_3-\text{MgO}$  plot (Irvine and Baragar, 1971), the mafic rocks show tholeiitic trend (Figure 4b). The diagram

presented by Peccerillo and Taylor (1976) indicates that the mafic rocks are low-to-medium K in nature, while the felsic rocks vary from high-K to shoshonitic (Figure 4c). Molar A/CNK values in the A/NK vs. A/CNK plot (Chappell and White, 1992) indicate that the dolerites of the Nimchak Pluton are metaluminous in nature, while the felsic rocks show peraluminous compositions with most of the samples representing S-type granites (Figure 4d).

### Trace elements

The representative analysis of trace and rare earth elements is listed in Table 1. Normalized to Primitive Mantle, the mafic and felsic rocks from the Nimchak Pluton show elevated values of large-ion lithophile elements (LILE) with respect to high-field strength

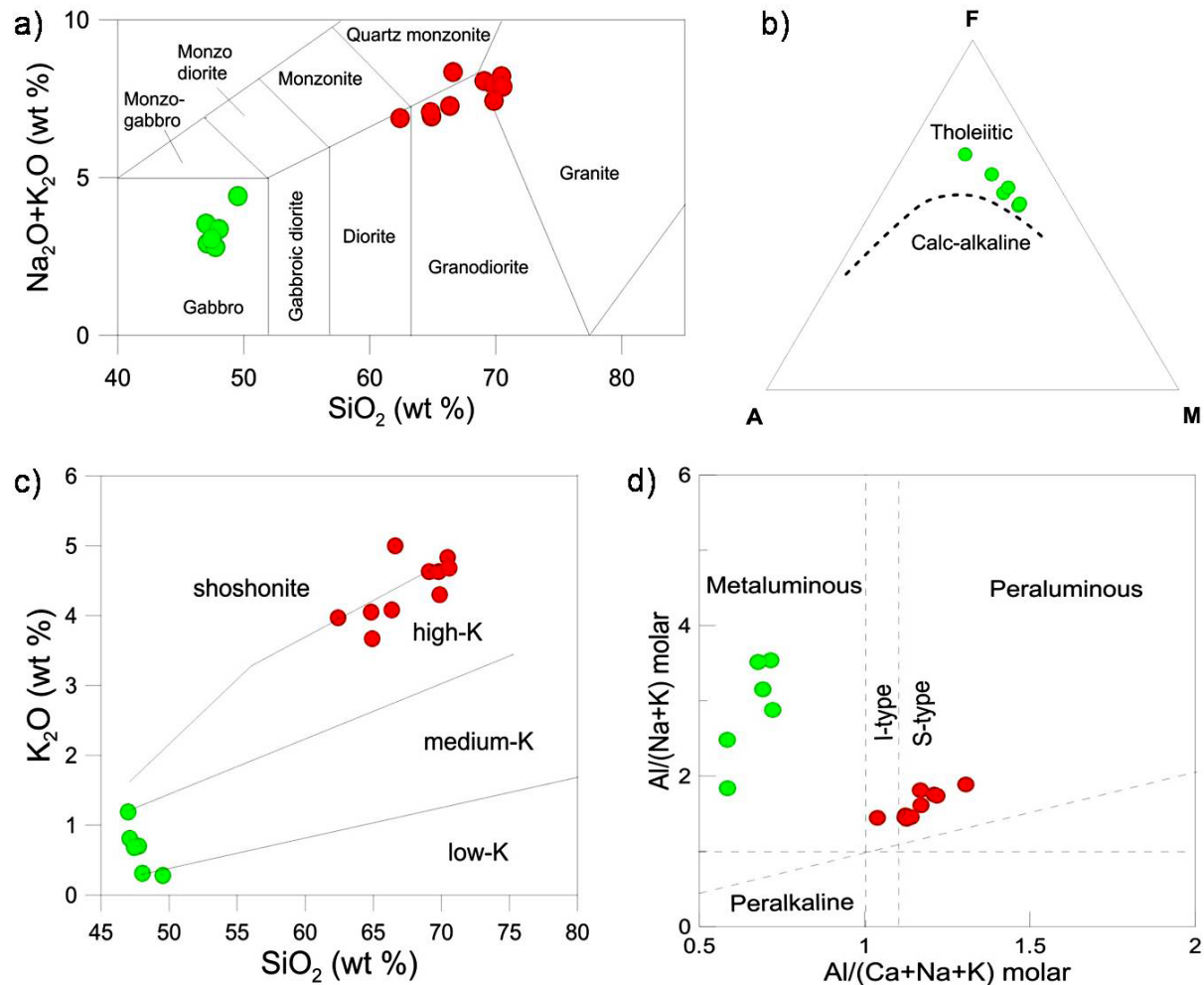


Figure 4. a) Total Alkali Silica plot displaying the geochemical nomenclature of the mafic and felsic rocks from NGP. b) AFM diagram displaying the nature of magma for the mafic rocks of NGP. c)  $\text{K}_2\text{O}$ - $\text{SiO}_2$  diagram showing that the mafic rocks are low- to medium-K in nature, while the felsic rocks vary from high-K to shoshonitic. d) Molar A/NK vs. A/CNK plot indicating the nature of the mafic and felsic rocks. Symbols represent: green circles - mafic rocks, red circles - felsic rocks.

Table 1. Representative major, trace and rare earth element compositions of the mafic and felsic rocks from the Nimchak Pluton [Some of the data are already published in Gogoi et al. (2018)].

Rock type	Mafic										Felsic									
	RD2C	RD30FM	RD30MC	RD30C	RD30DM	RD4	RD22	RD28	RD35	RD29F	RD25	RD39	RJ45	RJ48E	RD21	RD29C				
SiO <sub>2</sub>	47.00	49.54	48.04	47.11	47.77	47.44	69.09	69.80	70.47	70.57	69.87	62.42	66.61	66.36	64.92	64.84				
TiO <sub>2</sub>	1.89	2.99	2.50	1.43	1.50	2.06	0.22	0.26	0.21	0.21	0.25	0.74	0.32	0.50	0.57	0.63				
Al <sub>2</sub> O <sub>3</sub>	14.84	13.04	13.33	15.33	14.81	14.61	15.75	15.22	15.45	15.03	15.81	17.14	15.76	17.50	16.38	16.27				
Fe <sub>2</sub> O <sub>3</sub>	13.82	16.34	14.24	12.25	12.52	14.16	3.20	2.99	2.57	2.62	2.23	5.05	3.94	4.39	4.82	4.72				
MnO	0.18	0.21	0.20	0.17	0.18	0.20	0.08	0.07	0.06	0.06	0.02	0.09	0.08	0.04	0.04	0.05				
MgO	7.20	3.54	5.52	8.09	8.20	7.28	0.52	0.61	0.50	0.52	0.55	1.79	0.68	0.86	1.29	1.45				
CaO	8.47	8.35	9.59	9.39	9.71	9.06	1.85	1.69	1.61	1.57	2.04	2.22	2.35	2.92	2.31	2.20				
Na <sub>2</sub> O	2.35	4.13	3.06	2.10	2.10	2.37	3.43	3.33	3.38	3.20	3.13	2.91	3.34	3.19	3.26	3.02				
K <sub>2</sub> O	1.19	0.28	0.31	0.81	0.70	0.68	4.63	4.63	4.83	4.68	4.30	3.97	5.00	4.08	3.67	4.05				
P <sub>2</sub> O <sub>5</sub>	0.25	0.44	0.27	0.19	0.15	0.22	0.15	0.15	0.13	0.13	0.11	0.54	0.14	0.11	0.14	0.17				
LOI	2.04	1.60	1.66	2.14	2.12	1.40	0.80	0.81	0.80	0.85	0.78	1.27	1.11	0.84	1.57	1.62				
Total	99.23	100.46	98.72	99.01	99.76	99.48	99.72	99.56	100.01	99.44	99.09	98.14	99.33	100.79	98.97	99.02				
Ba	0	0	0	12	32	0	429	461	442	456	984	1548	746	1206	1030	1187				
Co	1032	0	1850	1573	1029	3067	9	2	7	4	7	15	147	74	15	8				
Cr	132	92	148	204	222	165	187	201	220	178	184	156	4	21	195	184				
Cu	36	42	111	46	49	36	5	4	6	4	9	8	8	8	13	4				
Ga	18	20	19	15	17	15	17	22	19	18	18	25	18	19	21	24				
Nb	13	24	12	9	10	12	22	21	17	23	14	51	18	27	25	26				
Ni	79	4	25	102	99	75	3	4	1	0	2	11	1	9	9	7				
Pb	3	4	1	2	6	7	41	35	43	43	35	22	37	22	28	27				
Rb	73	12	31	58	56	56	354	346	292	322	145	302	293	210	188	215				
Sc	25	33	37	32	39	22	0	8	13	0	18	15	7	8	27	6				
Sr	280	148	225	259	222	215	162	177	157	157	219	196	183	238	186	189				
Th	3	4	2	4	2	0	5	37	34	31	23	37	33	37	42	43				
U	1	1	1	1	1	2	6	10	8	11	0	3	6	4	0	29				

Table 1. ...Continued

Rock type	Mafic										Felsic									
	RD2C	RD30FM	RD30MC	RD30C	RD30DM	RD4	RD22	RD28	RD35	RD29F	RD25	RD39	RJ45	RJ48E	RD21	RD29C				
V	270	344	484	236	254	328	11	13	12	12	20	63	21	51	49	68				
Y	31	45	28	26	28	30	47	46	40	41	12	44	30	24	23	32				
Zn	106	65	73	95	94	111	45	48	61	45	30	70	51	83	64	68				
Zr	120	208	127	97	98	117	151	177	141	150	178	383	167	294	349	327				
La	12.5	26.6	13.9	9.3	10.3	13.4	37.9	36.4	37.1	34.9	85.1	94.1	67.3	134	95.6	79.4				
Ce	29.6	63.2	33.5	22.2	24.5	31.8	86.5	84.2	85.6	81.0	210.5	234.5	129.2	264.8	239.5	197.8				
Pr	4.2	8.9	4.8	3.2	3.5	4.5	9.5	9.0	9.2	8.5	23.9	27.4	12.9	27.3	28.2	22.1				
Nd	18.3	38.7	21.8	14.0	15.4	19.7	36.5	32.9	34.1	32.0	94.7	114.5	47.7	102.0	114.5	87.9				
Sm	4.52	9.24	5.62	3.58	3.89	4.79	8.5	7.79	7.84	7.50	21.04	25.4	6.79	15.31	25.5	20.2				
Eu	1.61	2.98	1.96	1.26	1.36	1.59	0.09	0.09	0.08	0.08	0.23	0.28	0.92	1.95	0.27	0.22				
Gd	4.92	10.17	6.29	3.96	4.34	5.32	4.79	4.25	4.05	4.26	10.53	12.51	5.37	11.76	12.36	10.2				
Tb	0.77	1.66	1.04	0.65	0.70	0.84	0.85	0.74	0.71	0.73	1.54	1.91	0.75	1.46	1.79	1.61				
Dy	4.61	9.69	6.19	3.86	4.16	5.05	4.3	3.91	3.45	3.59	5.19	6.99	4.37	6.53	5.96	5.29				
Ho	0.95	1.99	1.29	0.80	0.86	1.05	0.8	0.73	0.60	0.64	0.71	1.02	0.76	0.95	0.81	0.77				
Er	2.48	5.24	3.35	2.10	2.23	2.70	2.13	2.00	1.54	1.70	1.64	2.41	1.81	1.75	1.83	1.83				
Tm	0.36	0.78	0.50	0.31	0.34	0.40	0.34	0.32	0.25	0.26	0.19	0.32	0.31	0.21	0.22	0.24				
Yb	2.33	5.10	3.24	2.01	2.11	2.51	2.33	2.22	1.56	1.69	0.99	1.81	2.12	1.26	1.12	1.26				
Lu	0.34	0.75	0.47	0.29	0.31	0.36	0.40	0.50	0.37	0.38	0.20	0.41	0.35	0.20	0.24	0.27				

Major elements are given in wt %, trace and rare earth elements in ppm, LOI is Loss on ignition

elements (HFSE). The rocks display moderate to high LILE/HFSE ratios (Figure 5 a,c). The mafic rocks display positive Pb and negative Nb anomalies signifying crustal assimilation during magma evolution. Two mafic samples show pronounced Ba negative anomalies, which may be possibly due to the effect of sub-solidus alteration. Besides, the felsic rocks display positive Pb and negative Nb aberrations suggesting crustal involvement in the origin of the felsic magma. The depletion of Ba, Sr and Eu suggests plagioclase fractionation during magma evolution or the occurrence of plagioclase feldspar in the source. Negative aberrations for Ti and P may be explained by the removal of Ti-rich phases like titanite or ilmenite and apatite during magma evolution.

The mafic and felsic rocks of the Nimchak Pluton show elevated values of light rare earth elements (LREE) in comparison to heavy rare earth elements (HREE). Normalized to Chondrite, the dolerites display fractionated REE patterns marked by LREE enrichment and slightly fractionated HREE patterns (Figure 5b). The sub-parallel

REE trends displayed by the dolerite samples from the two late-stage dykes suggest that they are differentiated products of the same parental magma. Meanwhile, normalized to Chondrite, the granites are marked by gentle to heavily fractionated LREE and gently fractionated to flat HREE (Figure 5d). The felsic rocks display strong negative Eu anomalies indicating fractionation of plagioclase either in the magma or in the solid residue. The sub-parallel REE trends displayed by the felsic rocks signify that they are differentiated products of the same parental magma, which is evident from field observations.

#### GEOCHRONOLOGY

The granitic rocks of the Nimchak Pluton contain monazite as an accessory mineral (Figure 6a). A total of eighteen point data analyses of monazite were obtained to estimate the crystallization age of the granitic rocks. The ThO<sub>2</sub> content in monazite varies between 2.30 and 5.62 wt%, UO<sub>2</sub> content varies between 0.02 and 0.23 wt% and PbO concentration varies from 0.18 to 0.50 wt% (Table

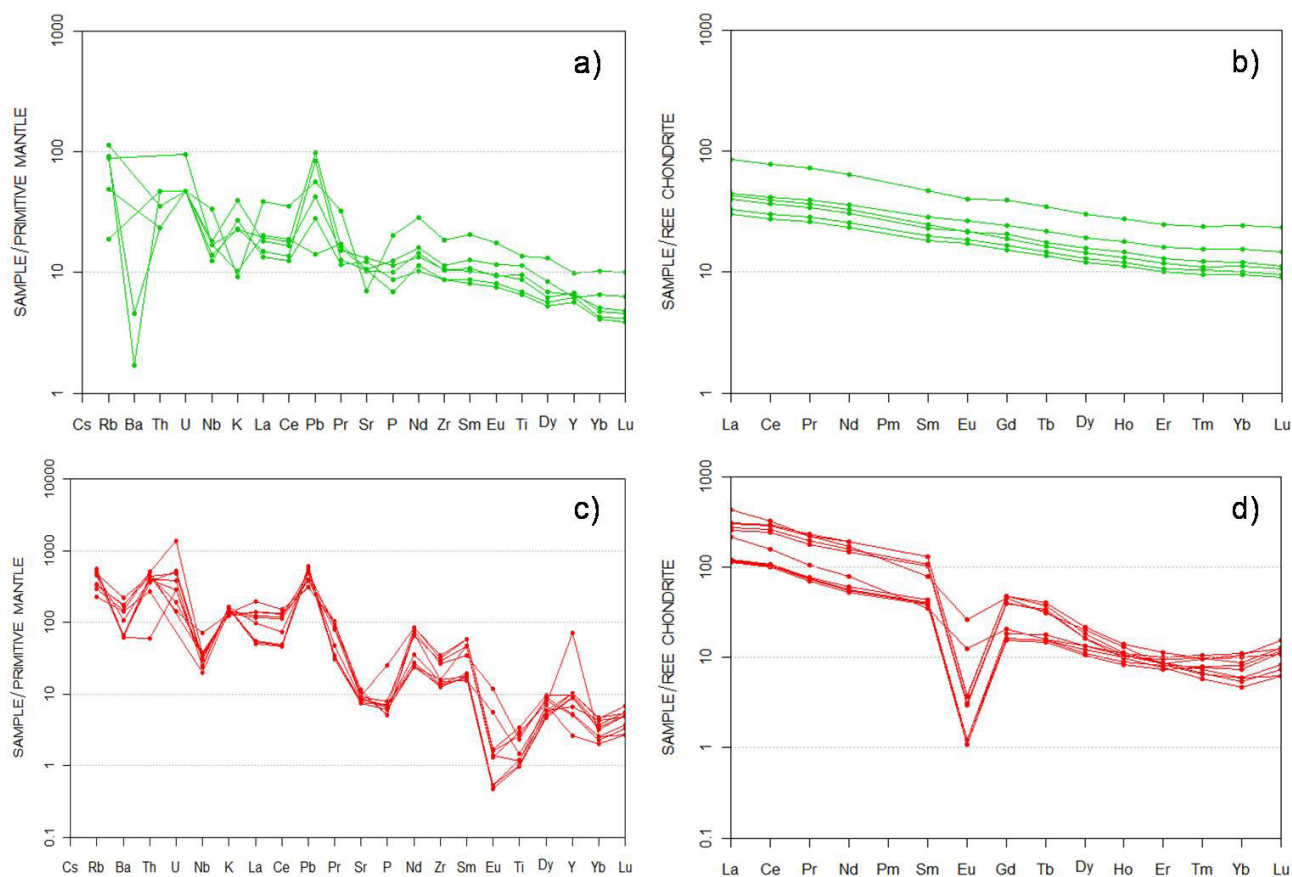


Figure 5. Primitive mantle normalized multi-element and chondrite normalized rare earth element patterns for the representative rock samples of NGP. a, b) Mafic rocks. c, d) Felsic rocks. Normalizing values of primitive mantle are after Sun and McDonough (1989) and those of chondrite are after Boyton (1984).

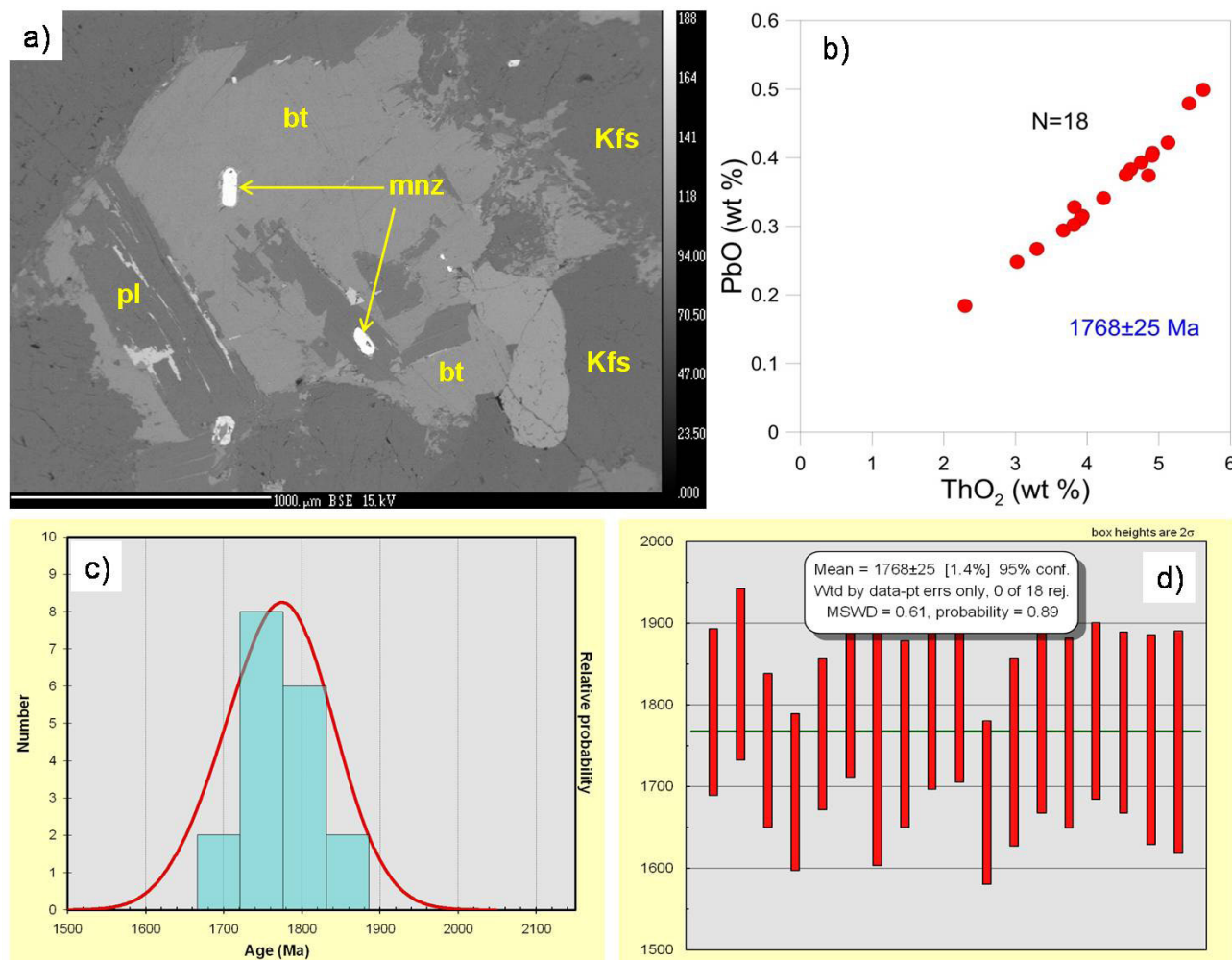


Figure 6. a) Back scattered electron image of granite displaying the occurrence of monazite along with other silicates. b) PbO vs ThO<sub>2</sub> plot of analytical data of monazite. c) Histogram of age data of Nimchak granite displaying peak around 1750 Ma. d) Weighted mean age with 2 sigma errors of monazite displaying 1768 Ma age for Nimchak granite.

2). Despite such variations in oxide concentrations in the mineral, uniform PbO/ThO<sub>2</sub> ratios (Figure 6b) were obtained within an age range of 1680-1837 Ma, which suggests that the crystallization of monazite is related to a single thermal event. The details of Th-U-Pb monazite age dating are illustrated in Figures 6c and 6d. A Th-U-Pb monazite age of 1768 ± 25 Ma is derived from the granites of the Nimchak Pluton that indicates the time of its emplacement.

## DISCUSSION

### Petrogenesis of the felsic and mafic rocks of the Nimchak Pluton

The dolerites from the Nimchak Pluton do not represent mantle-derived primary magmas as indicated by depleted Mg# (0.18-0.40), MgO (3.54-8.20 wt%), Cr (92-222 ppm) and Ni (4-102 ppm) contents. These signatures

suggest that the dolerites are fractional crystallization products of parental mafic magmas. The occurrence of clinopyroxene as the major mafic mineral and lack of olivine in the dolerites also support their differentiated nature. Normalized to Primitive Mantle, the dolerites display positive anomalies for Pb and negative anomalies for Nb indicating some amount of crustal assimilation. However, the absence of definite correlativity between Nb/La vs SiO<sub>2</sub> (Figure 7a) and Nb/La vs MgO (Figure 7b) contradict extensive crustal assimilation, as crustal assimilation would result in inversely correlated trends for Nb/La and SiO<sub>2</sub> and direct correlated trends for Nb/La and MgO (Jiang et al., 2019). Concentrations of Ni and Zr were used for evaluating mantle melting. On the Ni vs. Zr model (Condie et al., 1987), most of the dolerites indicate that they are products from a parental magma produced by

Table 2. Microprobe analysis of monazite from the granitic rocks, Nimchak Pluton

Analysis no.	SiO <sub>2</sub>	P <sub>2</sub> O <sub>5</sub>	ThO <sub>2</sub>	CaO	Y <sub>2</sub> O <sub>3</sub>	La <sub>2</sub> O <sub>3</sub>	Ce <sub>2</sub> O <sub>3</sub>	Pr <sub>2</sub> O <sub>3</sub>	Nd <sub>2</sub> O <sub>3</sub>	SmO	Gd <sub>2</sub> O <sub>3</sub>	Dy <sub>2</sub> O <sub>3</sub>	PbO	UO <sub>2</sub>	K <sub>2</sub> O	Total	Age (Ma)	2-sigma error (Ma)
1	0.44	28.39	4.92	1.10	1.34	14.35	27.30	3.38	10.37	1.62	1.14	0.27	0.41	0.07	0.00	95.08	1791	102
2	0.48	28.28	4.61	0.86	1.11	14.95	27.86	3.43	10.46	1.57	1.04	0.22	0.38	0.04	0.01	95.30	1837	105
3	0.75	27.80	5.43	0.85	1.15	15.19	28.03	3.28	9.52	1.46	0.97	0.24	0.48	0.23	0.01	95.37	1744	94
4	0.87	25.59	5.13	0.67	1.08	14.71	26.32	3.05	8.79	1.35	0.91	0.20	0.42	0.15	0.01	89.24	1693	96
5	0.42	28.34	5.62	1.12	1.63	14.01	27.32	3.34	9.93	1.66	1.23	0.32	0.50	0.22	0.02	95.68	1764	93
6	0.44	28.68	3.82	0.68	1.30	14.68	28.62	3.55	10.63	1.65	1.19	0.23	0.33	0.07	0.01	95.89	1830	119
7	0.35	28.68	2.30	0.47	0.58	15.71	30.72	3.76	11.30	1.48	0.96	0.12	0.18	0.02	0.00	96.64	1764	161
8	0.54	28.37	3.93	0.63	0.72	15.01	29.02	3.53	11.07	1.62	1.00	0.16	0.32	0.04	0.01	95.97	1764	114
9	0.44	28.67	4.76	0.88	1.26	14.57	27.78	3.55	10.50	1.66	1.14	0.32	0.39	0.06	0.01	95.98	1801	105
10	0.52	28.64	4.91	0.86	1.13	14.70	28.13	3.44	10.75	1.68	1.07	0.25	0.40	0.05	0.00	96.52	1808	103
11	0.52	28.65	4.86	0.96	1.22	14.39	27.96	3.35	10.45	1.70	1.16	0.29	0.37	0.06	0.00	95.94	1680	100
12	0.58	28.39	3.91	0.92	0.84	15.18	29.10	3.49	10.90	1.57	1.06	0.18	0.31	0.04	0.00	96.47	1742	115
13	0.59	28.50	3.67	0.89	0.69	15.40	29.10	3.57	10.76	1.47	1.01	0.10	0.29	0.02	0.00	96.07	1785	118
14	0.66	27.98	3.82	0.63	0.57	15.53	28.87	3.56	10.95	1.38	0.99	0.11	0.30	0.03	0.00	95.37	1765	116
15	0.57	28.36	4.54	0.97	1.16	14.34	28.01	3.49	10.52	1.74	1.20	0.25	0.38	0.06	0.00	95.59	1792	108
16	0.74	28.10	4.23	0.76	0.71	15.27	28.32	3.43	10.66	1.51	1.00	0.20	0.34	0.04	0.02	95.31	1778	111
17	0.48	27.59	3.30	0.66	1.16	14.80	29.55	3.69	11.27	1.87	1.31	0.29	0.27	0.05	0.00	96.29	1757	128
18	0.52	28.41	3.02	0.67	1.08	14.27	29.04	3.62	11.09	1.89	1.27	0.28	0.25	0.06	0.00	95.46	1754	136

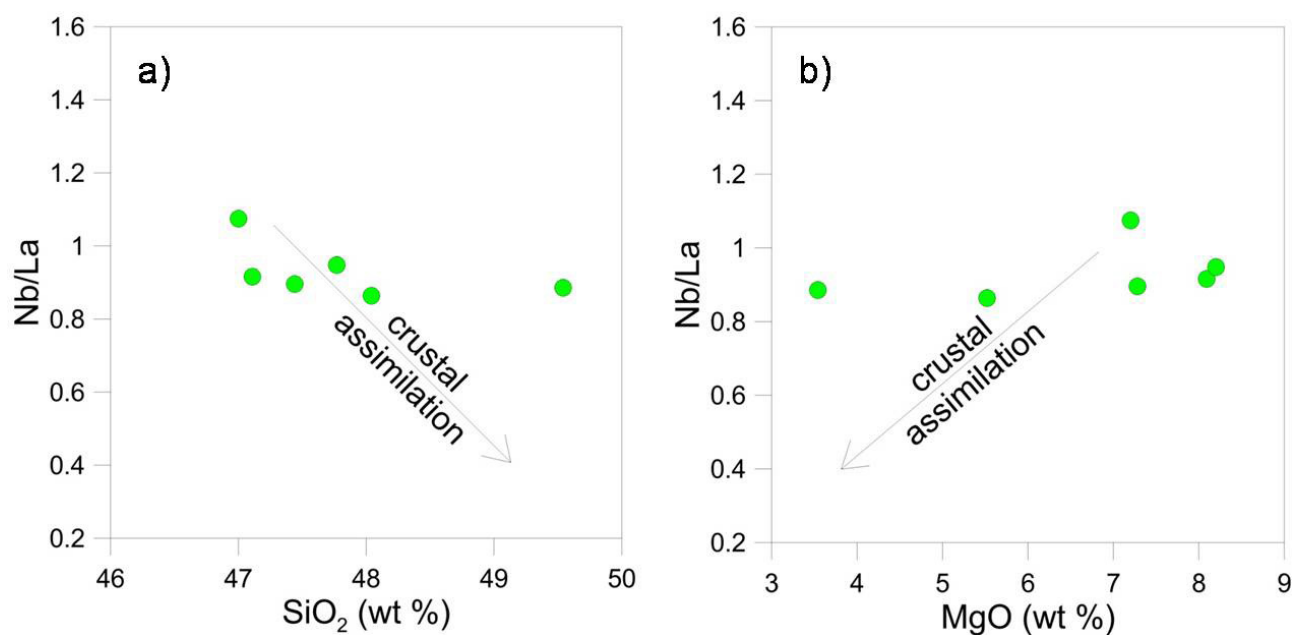


Figure 7. Plots for the mafic rocks of Nimchak Pluton. (a) SiO<sub>2</sub> vs Nb/La (b) MgO vs Nb/La.

12% to 15% melting of a lherzolite mantle source (Figure 8a). Moreover, in the Sm/Yb vs. La/Yb plot, the dolerites cluster between the melting curves of spinel lherzolite and spinel-garnet lherzolite with primitive mantle as starting composition (Figure 8b). The Sm/Yb values of the dolerites cluster below the garnet lherzolite melting curve but above the spinel lherzolite melting curve. This indicates that the dolerites are products of parental mafic magma that was possibly generated from a lherzolite mantle source consisting of spinel and minor garnet. Moreover, a ca. 10% partial melting of the lherzolite mantle source is required to produce the parental magma of the doleritic rocks. Thus, from the Ni vs. Zr and Sm/Yb vs. La/Yb plots, it can be ascertained that the parental magma of the mafic rocks from the Nimchak Pluton was produced by around 10% to 15% partial melting of a lherzolite mantle source.

The granitic rocks of the Nimchak Pluton are two-mica granites and, based on their high alumina saturation index (ASI) or A/CNK values, are defined as peraluminous S-type granites (Figure 4d), thus derived from partial melting of a metasedimentary source (Bonin, 2007). The nature of the crustal source of the granitic rocks can be determined with the help of their trace element characteristics. In the La/Yb vs. Sr/Y diagram (Wang et al., 2016), the granitic rocks of the Nimchak Pluton plot in the region of F2 and F3 (Figure 9). The felsic rocks display low Sr/Y (<20) and variable La/Yb ratios. These features suggest that the Nimchak granites were produced

by partial melting of a plagioclase-rich and garnet-poor source at relatively low pressures (Gao et al., 2017).

#### Geotectonic framework

The mafic and felsic rocks of the Nimchak Pluton display high LILE/HFSE and LREE/HREE ratios, which are distinctive features of magmas generated in subduction zones (Hawkesworth et al., 1993; Gorton and Schandl, 2000). On the tectonic discrimination diagrams (Figure 10), the dolerites from the late-stage mafic dykes distinctly plot in the region of 'back-arc basin basalt'. Thus, the magmas that fed the dolerite intrusions in the Nimchak Pluton were produced in a back-arc extensional setting associated with subduction dynamics. Moreover, on the tectonic discrimination diagrams, the granites of the Nimchak Pluton also cluster in the region of 'typical arc rocks' generated in a subduction zone setting (Figure 11). These results suggest that the mafic and felsic rocks of the Nimchak Pluton were produced in a back-arc extensional setting. Thus, the BVSs represents a back-arc rift basin.

The Nimchak Pluton is a ca. 1 km<sup>2</sup> granitoid body within the BVSs. Field observations suggest that this granitic body was intruded by at least eight mafic/dolerite dykes during the entire crystallization/solidification period of the felsic reservoir (Gogoi et al., 2017; Gogoi et al., 2018; Gogoi et al., 2020). This clearly suggests that the BVSs witnessed extensive mafic dyke emplacement during its evolution, which further validates the fact that the volcano-sedimentary suite developed in a rift setting.

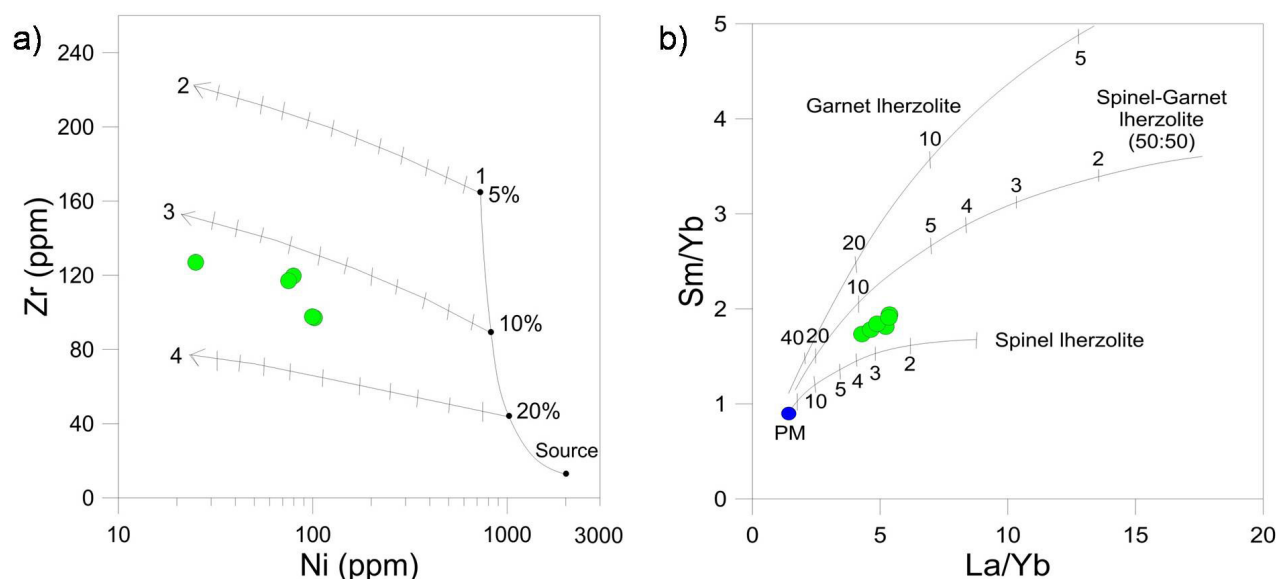


Figure 8. Plots for the mafic rocks of Nimchak Pluton. a) Petrogenetic model based on Ni vs Zr for a lherzolite mantle composition (2000 ppm Ni and 11 ppm Zr). Curve 1 represents batch melting at 1500 °C (1 atm. equivalent) with degrees of melting displayed in percentages. Curves 2, 3, and 4 illustrate olivine fractionation with removal of olivine noted in 5% increments (after Condie et al., 1987). b) La/Yb vs Sm/Yb plot (after Liu et al., 2014). PM - Primitive Mantle.

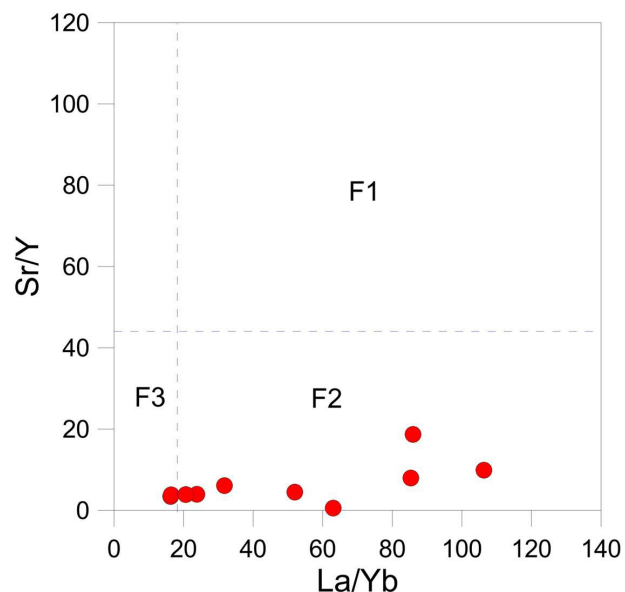


Figure 9. La/Yb vs Sr/Y plot for the felsic rocks of Nimchak Pluton that illustrates the role of residual garnet and plagioclase during partial melting. F1 - field of adakitic melts derived from partial melting of eclogites in the stability field of garnet with little or no plagioclase, F2- field of crustal melts in the stability field of garnet and plagioclase, F3 - field of crustal melts in the stability field of plagioclase with little or no garnet.

The Sr-Nd isotope ratios presented by Gogoi et al. (2020) suggest that the dolerites and granites of the Nimchak Pluton are not genetically related. This indicates that the felsic endmember of our study domain is not a fractional crystallization product of the mafic magma. As such, crustal anatexis induced by the high-temperature mafic magma seems to be the favourable mechanism for the origin of the NGP. Upwelling of the asthenosphere caused formation of mafic magmas in the upper mantle beneath the BVSs. After their formation, the mafic magmas began to rise, perhaps through diapirism or through faults and fractures, eventually underplating at the base of the crust. The underplating of the mafic magmas initiated partial melting in the overlying crustal rocks producing granitic magma chambers therein. These chambers were later intruded by the underlying mafic magmas, which are now preserved as mafic dykes within the granitic plutons.

#### Tectonomagmatic evolution of the CGGC

As already discussed earlier, the tectonomagmatic evolution of CGGC is highly debated. This is due to the lack of meaningful geological and geochronological information from most parts of CGGC (Sanyal and Sengupta, 2012). To make matters worse, most of the lithological associations from this mobile belt have undergone metamorphism. This makes BVSs a very strong geological entity to reveal the tectonomagmatic evolution of CGGC as it happens to be the first reported

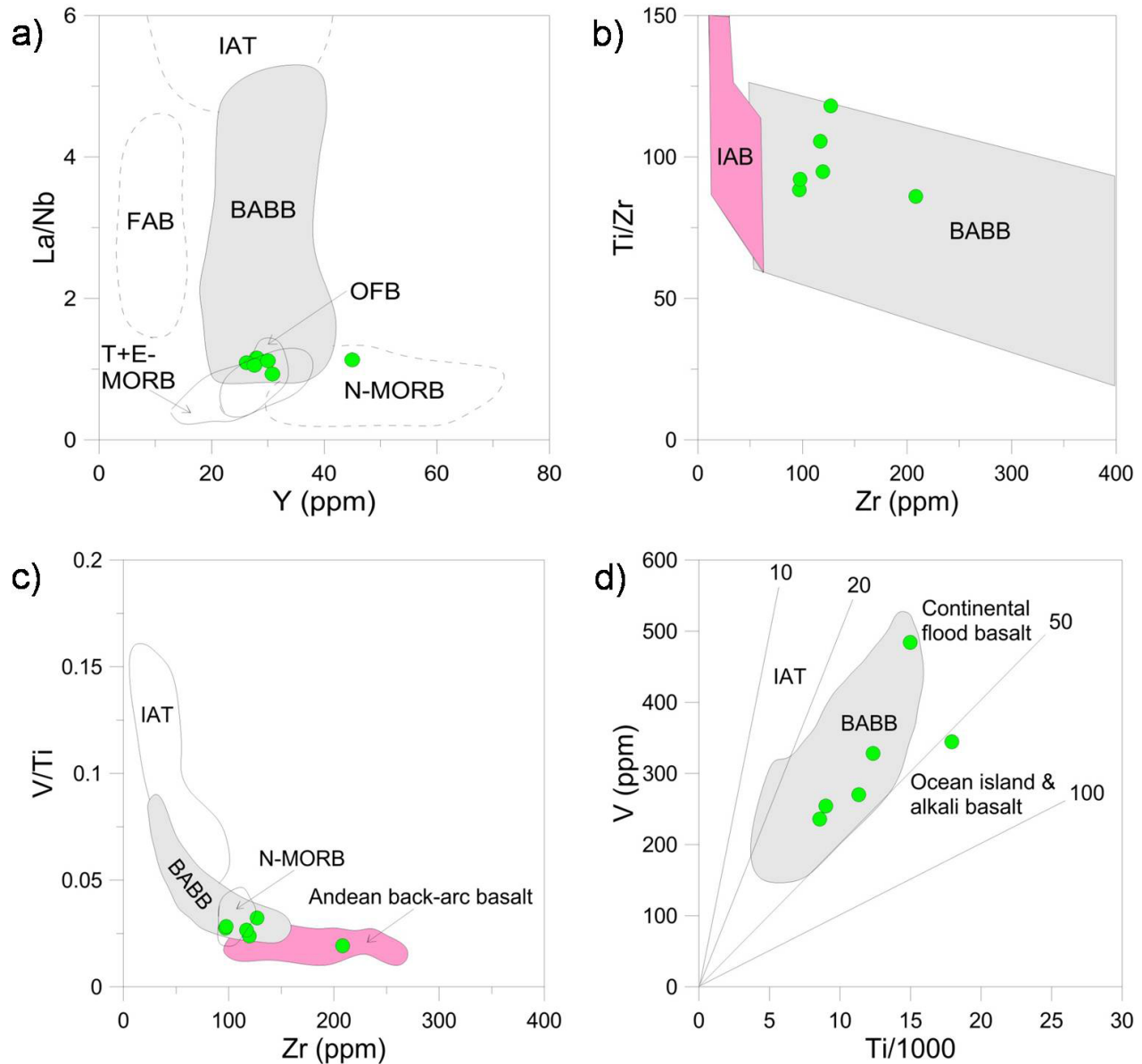


Figure 10. Tectonic discrimination diagrams for the mafic rocks of Nimchak Pluton. a) La/Nb vs Y (after Floyd et al., 1991). b) Ti/Zr vs Zr (after Woodhead et al., 1993). c) Zr vs V/Ti (after Woodhead et al., 1993). d) V vs Ti/1000 (after Pearce, 2014). Field of Andean back-arc basalt is from Espanon et al. (2014). BABB - Back-arc basin basalt, FAB - Fore-arc basalt, IAB - Island arc basalt, IAT - Island arc tholeiites, OFB - Ocean floor basalt.

magmatic suite of rocks from the northern margin of the gneissic terrain.

From the results presented in this work it is quite evident that the BVSs evolved in a back-arc extensional setting during ca. 1700 Ma. This age conforms to the U-Pb (ID-TIMS) zircon emplacement age of ca. 1700-1600 Ma for the granites of the BVSs (Saikia et al., 2017). It can be argued that the mafic dykes are not comagmatic and intruded the granitic rocks during a later tectonothermal

event. However, there is strong evidence that most of the mafic dykes preserved in the Nimchak Pluton intruded the granitic magma chamber at different stages of its crystallization history (Gogoi et al., 2017; Gogoi et al., 2018; Gogoi et al., 2020). The occurrence of only two late-stage mafic dykes in the granitic pluton would have made this work complicated. However, there is evidence of at least six other mafic dykes that intruded the Nimchak Pluton at various stages of its crystallization and interacted

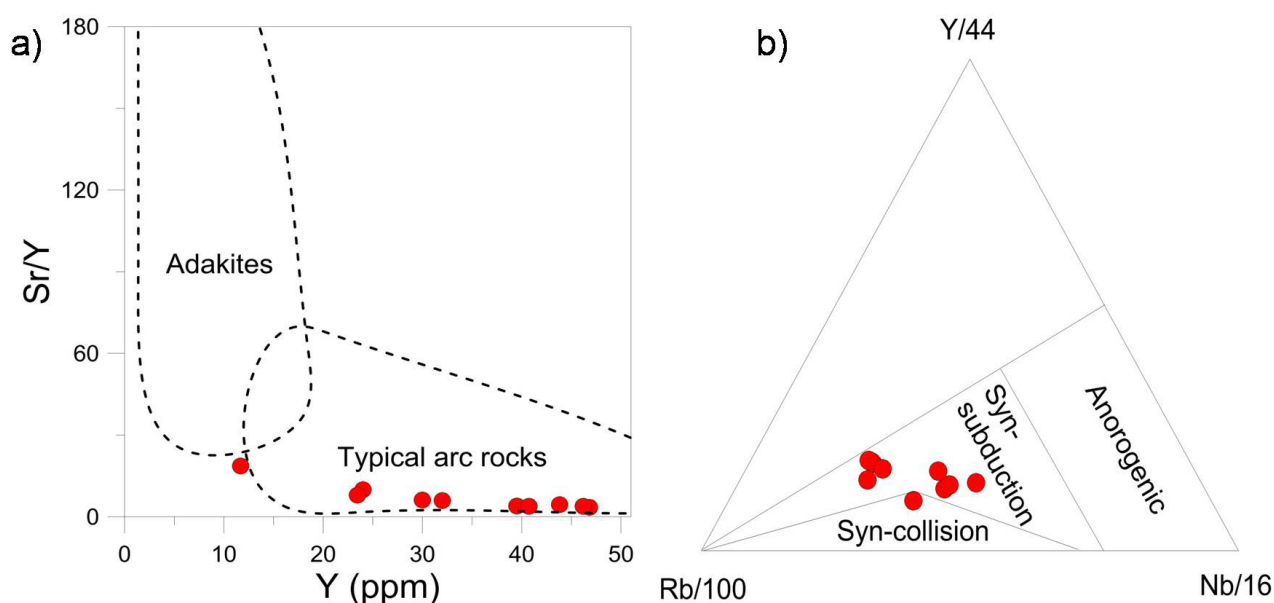


Figure 11. Tectonic discrimination diagrams for the felsic rocks of Nimchak Pluton. a) Sr/Y vs Y plot (after Defant and Drummond, 1990). b) Y/44-Rb/100-Nb/16 plot (after Thieb̄lemont and Cabanis, 1990).

with the granitic magma. Such field observations clearly demonstrate that the two late-stage mafic dykes preserved in the Nimchak Pluton are synplutonic in nature. Moreover, the composition of mafic rocks from the two late-stage mafic dykes matches with the composition of mafic rocks from other parts of the BVSs (Gogoi et al., 2020). Such compositional similarities suggest that the two late-stage mafic dykes preserved in the Nimchak Pluton are related to the Bathani magmatism.

The DVB is an arcuate linear belt located to the south of the CGGC. Although the geodynamic evolution of Dalma volcanics is highly debated, one school of thought suggests an island arc tectonic setting for the origin and evolution of the DVB (Naha and Ghosh, 1960; Alvi et al., 2019; Chakraborty et al., 2019). The Dalma volcanics are generally considered to be Palaeoproterozoic in age (1740-1630 Ma; Reddy et al., 2009; Mazumder et al., 2012; Chatterjee et al., 2013). On the other hand, the BVSs is a linear back-arc rift basin located to the north of the CGGC. Similar to the DVB, the BVSs is also considered to be Palaeoproterozoic in age (ca. 1700-1600 Ma; Saikia et al., 2017; Saikia et al., 2019). The existence of these two contemporaneous subparallel belts offers new perspective for the tectonomagmatic evolution of the CGGC during the Proterozoic. The occurrence of BVSs in northern CGGC and DVB in southern CGGC can be explained by northward subduction of the Singhbhum Craton beneath the Bundelkhand Craton. The arcuate nature of the DVB further supports this model. However, it is to be noted

here that the subduction mechanism occurred between two oceanic plates. Thus, two oceanic plates were attached to the two cratonic blocks; one oceanic plate was attached to the northern margin of the Singhbhum Craton, while the other was attached to the southern margin of the Bundelkhand Craton. The oceanic plate attached to the Singhbhum Craton underwent subduction beneath the oceanic plate of the Bundelkhand Craton to produce a volcanic arc and a back arc on the latter. The volcanic arc is represented by the DVB located to the south of the CGGC, while the back arc is represented by the BVSs located to the north of CGGC. A tectonomagmatic model for the origin of the DVB and BVSs and evolution of the CGGC during the Proterozoic is showcased in Figure 12.

#### Implications for the Columbia supercontinent formation

India has always been an integral part of the Columbia supercontinent build-up models (Meert, 2002; Rogers and Santosh, 2002; Zhao et al., 2002; Hou et al., 2008; Pesonen et al., 2012; Zhang et al., 2012; Pisarevsky et al., 2013). It is inferred that the Columbia supercontinent amalgamated at around 1900-1600 Ma and fragmented during 1500-1200 Ma (Hoffman, 1989; Evans, 2013). However, the position of India in the various hypothesized models has remained speculative because of the lack of sufficient geochronological and palaeomagnetic data from the Indian landmass. In the model presented by Hou et al. (2008), India was positioned close to Laurentia and North China Craton, Zhang et al. (2012) placed it close to

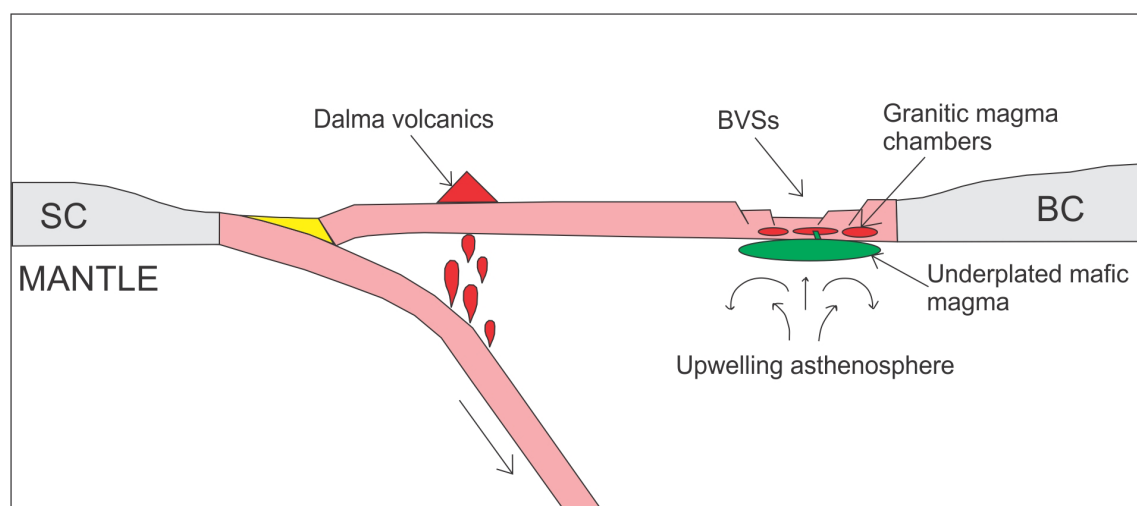


Figure 12. A simplified tectonomagmatic model for the origin of the Dalma volcanics and Bathani volcano-sedimentary sequence and evolution of the CGGC during the Proterozoic (see text for more details). BC - Bundelkhand Craton, BVSS - Bathani volcano-sedimentary sequence, SC - Singhbhum Craton.

Australia and Pisarevsky et al. (2013) placed it near the Sarmatia margin of Baltica. Thus, the location of India within the Columbia supercontinent varies substantially in the recently hypothesized models.

The CGGC is an integral part of the Central Indian Tectonic Zone, which is a ca. 1500 km mobile belt within the Indian landmass that marks the suturing of the northern and southern crustal provinces to form the Greater Indian Landmass during the Proterozoic. The northern crustal province consists of the Archaean Bundelkhand Craton as its nucleus, while the southern province is a composite assemblage of the Dharwar, the Bastar and the Singhbhum Archaean Cratons. However, the mechanism and timing of suturing between the northern and southern crustal domains remain speculative till date. The various hypothesized models proposed for the amalgamation of the Greater Indian Landmass include northward subduction of the southern block beneath the northern block with continental collision at ca. 1500 Ma (Roy and Prasad, 2003), southward subduction of the northern block beneath the southern block during 2100-1800 Ma (Yedekar et al., 1990; Jain et al., 1991; Mishra et al., 2000), rifting in the northern margin of the southern crustal province at ca. 1400 Ma followed by merger of the two blocks at ca. 1100 Ma (Roy et al., 2006), continental subduction followed by collisional thickening at >1500 Ma (Mahato et al., 2008), double-sided subduction phenomenon at ca. 1600 Ma (Naganjaneyulu and Santosh, 2010) and arc-continent collision between 1570 and 1540 Ma (Bhowmik et al., 2012). The results presented in this work justify that the Greater Indian Landmass was formed due to northward

subduction of the southern crustal province beneath the northern crustal province at around 1700 Ma. A recent work by Chakraborty et al. (2019) also supports this model. The reported age further justifies that the Greater Indian Landmass amalgamated during the formation of the Columbia supercontinent. This suggests that India was not a single continental block as portrayed in most of the hypothesized models of the Columbia supercontinent formation (Rogers and Santosh, 2002; Zhao et al., 2002; Hou et al., 2008; Zhang et al., 2012; Pisarevsky et al., 2013). The Greater Indian Landmass was formed during the assembly of Columbia between 1900 Ma and 1600 Ma. It seems highly probable that the Central Indian Tectonic Zone was a part of the adjoining proto-continental blocks that were attached to the eastern and western margins of India in the Columbia supercontinent. After fragmentation of Columbia or a later supercontinent, India separated from the other continental blocks. However, the eastward and westward extensions of the Central Indian Tectonic Zone must be preserved in those blocks. Thus, it will be fruitful to look for continuation of mobile belts similar in nature to the Central Indian Tectonic Zone in the adjoining proto-continental blocks while placing India in the Columbia supercontinent formation.

## CONCLUSIONS

- The Bathani volcano-sedimentary sequence, which is the eastern extension of the Mahakoshal Mobile Belt, represents a back-arc rift setting. Th-U-Pb monazite dating gives a formation age of ca. 1700 Ma for the BVSS.
- The CGGC represents an island arc setting in

which the Dalma volcanics represent the volcanic arc, while the BVSS represents the back-arc rift. Subduction of the southern Singhbhum block beneath the northern Bundelkhand block during the Proterozoic produced the island arc system. The crustal plates involved in this subduction were oceanic plates that were attached to the Singhbhum and Bundelkhand cratons.

c) The Greater Indian Landmass amalgamated due to northward subduction of the southern crustal province beneath the northern crustal province during the Columbia supercontinent formation.

d) India was not a single continental block during the Columbia supercontinent formation. The occurrence of mobile belts similar in nature to the Central Indian Tectonic Zone in the adjoining proto-continental blocks should be considered while placing India within Columbia.

#### ACKNOWLEDGEMENTS

Constructive reviews by two anonymous reviewers have significantly improved the quality of the manuscript. The author is grateful to Section Editor Orlando Vaselli for handling the manuscript. The author is also grateful to his supervisor Ashima Saikia for the geochemical and geochronology data used in this work. The author acknowledges the CSIR grant vide Project no. 24(0317)/12/EMR-II and CSIR JRF/SRF fellowship no. 09/045(1146)/2011-EMR1.

#### REFERENCES

- Acharyya S.K., 2003. The nature of Mesoproterozoic central Indian tectonic zone with exhumed and reworked older granulites. *Gondwana Research* 6, 197-214.
- Ahmad M. and Paul A.Q., 2013. Investigation of volcano-sedimentary sequence and associated rocks to identify gold and base metal mineralization at Gere-Kewti area of Gaya District, Bihar (G4). Geological Survey of India (F.S.: 2012-13) (Unpublished report).
- Ahmad M. and Wanjari N., 2009. Volcano-sedimentary sequence in the Munger-Rajgir metasedimentary belt, Gaya district, Bihar. *Indian Journal of Geoscience* 63, 351-360.
- Alvi S.H., Mir A.R., Bhat I.M., 2019. Geochemistry of Dalma metavolcanic Suite from Proterozoic Singhbhum Mobile Belt, Eastern India: Implications for Petrogenesis and Tectonic Setting. *Journal of the Geological Society of India* 94, 351-358.
- Balaram V., Saxena V.K., Manikyamba C., Ramesh S.L., 1990. Determination of rare earth elements in Japanese rock standards by inductively coupled plasma mass spectrometry. *Atomic Spectroscopy* 11, 19-23.
- Bhattacharya H., Nelson D., Thern E., Altermann W., 2015. Petrogenesis and geochronology of the Arkasani granophyre and felsic Dalma volcanic rocks: Implications for the evolution of the Proterozoic North Singhbhum Mobile Belt, east India. *Geological Magazine* 152, 492-503.
- Bhowmik S.K., Wilde S.A., Bhandari A., Pal T., Pant N.C., 2012. Growth of the Greater Indian landmass and its assembly in Rodinia: Geochronological evidence from the Central Indian Tectonic Zone. *Gondwana Research* 22, 54-72.
- Bonin B., 2007. A-type granites and related rocks: evolution of a concept, problems and prospects. *Lithos* 97, 1-29.
- Boyton W.V., 1984. Cosmochemistry of the rare earth elements: Meteorite studies. In: *Rare earth element geochemistry*. (Eds.): P. Henderson, Elsevier, Amsterdam, 63-114.
- Chakraborty T., Upadhyay D., Ranjan S., Pruseth K.L., Nanda J.K., 2019. The geological evolution of the Gangpur Schist Belt, eastern India: Constraints on the formation of the Greater Indian Landmass in the Proterozoic. *Journal of Metamorphic Geology* 37, 113-151.
- Chappell B.W. and White A.J.R., 1992. I- and S- type granites in Lachlan Fold Belt. *Transactions of the Royal Society of Edinburgh* 83, 1-26.
- Chatterjee P., De S., Ranaivoson M., Mazumder R., Arima R., 2013. A Review of the ~1600 Ma Sedimentation, Volcanism and Tectono-Thermal Events in The Singhbhum Craton, Eastern Indian Craton. *Geoscience Frontiers* 4, 277-287.
- Condie K.C., Bobrow D.J., Card K.D., 1987. Geochemistry of Precambrian mafic dikes from the southern Superior Province. In: *Mafic dike swarms*. (Eds.): H.C. Halls and W.F. Fahrig, Geological Association of Canada Special Paper 34, 95-108.
- Defant M.J. and Drummond M.S., 1990. Derivation of some modern arc magmas by melting of young subducted lithosphere. *Nature* 347, 662-665.
- Dora M.L., Singh Y., Joshi S., Kundu A., Suresh G., Randive K.R., 2019. The first report on the chemical (Th-U-Pb) monazite age of the Mul granite pluton, Western Bastar Craton, central India and its metallogenic significance. *Journal of Earth System Science* 128, 124.
- Espanon V.R., Chivas A.R., Kinsley L.P.J., Dosseto A., 2014. Geochemical variations in the Quaternary Andean back-arc volcanism, southern Mendoza, Argentina. *Lithos* 208-209, 251-264.
- Evans D.A.D., 2013. Reconstructing pre-Pangean supercontinents. *Geological Society of America Bulletin* 125, 1735-1751.
- Floyd P.A., Kelling G., Gocken S.L., Gocken N., 1991. Geochemistry and tectonic environment of basaltic rocks from the Miss ophiolitic melange, south Turkey. *Chemical Geology* 89, 263-280.
- Gao P., Zheng Y.F., Zhao Z.F., 2017. Triassic granites in South China: A geochemical perspective on their characteristics, petrogenesis, and tectonic significance. *Earth Science Reviews* 173, 266-294.
- Gogoi B., Saikia A., Ahmad M., 2020. Mafic-felsic magma interactions in the Bathani volcanic-plutonic complex of Chotanagpur Granite Gneiss Complex, eastern India: implications for assembly of the Greater Indian Landmass during the Proterozoic. *Episodes* 43, 785-810.

- Gogoi B., Saikia A., Ahmad M., 2017. Titanite-centered ocellar texture: a petrological tool to unravel the mechanism enhancing magma mixing. *Periodico di Mineralogia* 86, 245-273.
- Gogoi B., Saikia A., Ahmad M., 2018. Field evidence, mineral chemical and geochemical constraints on mafic-felsic magma interactions in a vertically zoned magma chamber from the Chotanagpur Granite Gneiss Complex of Eastern India. *Chemie der Erde-Geochemistry* 78, 78-102.
- Gorton M.P. and Schandl E.S., 2000. From continents to island arcs: a geochemical index of tectonic setting for arc-related and within-plate felsic to intermediate volcanic rocks. *The Canadian Mineralogist* 38, 1065-1073.
- Gupta A. and Basu A., 2000. North Singhbhum Proterozoic mobile belt, eastern India-A review. MS Krishnan Centenary Volume, Geological Survey India Special Publication 55, 195-226.
- Hawkesworth C.J., Gallagher K., Hergt J.M., McDermott F., 1993. Mantle and slab contributions in arc magmas. *Annual Reviews of Earth and Planetary Sciences* 21, 175-204.
- Hoffman P.F., 1989. Speculations on Laurentia's first Gigayear (2.0-1.0 Ga). *Geology* 17, 135-138.
- Hou G., Santosh M., Qian X., Lister G.S., Li J., 2008. Configuration of the Late Paleoproterozoic super continent Columbia: insights from radiating mafic dyke swarms. *Gondwana Research* 14, 395-409.
- Irvine T.N. and Baragar W.R.A., 1971. A guide to the geochemical classification of the common volcanic rocks. *Canadian Journal of Earth Sciences* 8, 523-548.
- Jain S.C., Yedekar D.B., Nair K.K.K., 1991. Central Indian shear zone: A major Precambrian crustal boundary. *Journal of the Geological Society of India* 37, 521-532.
- Jiang W., Yan Q., Deng L., Zhou B., Xiang Z., Xia W., 2019. Early Jurassic Mafic Intrusions in the Southern Youjiang Basin, SW China: Petrogenesis, Tectonic and Metallogenic Implications. *Minerals* 9, 771.
- Liu B., Ma C.Q., Zhang J.Y., Xiong F.H., Huang J., Jiang H.A., 2014.  $^{40}\text{Ar}$ - $^{39}\text{Ar}$  age and geochemistry of subduction-related mafic dikes in northern Tibet, China: petrogenesis and tectonic implications. *International Geology Review* 56, 57-73.
- Ludwig K.R., 2001. SQUID 1.02, A User Manual, a Geochronological Toolkit for Microsoft Excel. Berkeley, USA: Berkeley Geochronology Center Special Publication.
- Mahadevan T.M., 2002. *Geology of Bihar and Jharkhand*. Bangalore: Geological Society of India.
- Mahato S., Goon S., Bhattacharya A., Mishra B., Bernhardt H.J., 2008. Thermo-tectonic evolution of the North Singhbhum Mobile Belt: A view from the western part of the belt. *Precambrian Research* 162, 102-107.
- Mahato S., Goon S., Bhattacharya A., Mishra B., Bernhardt H.J., 2008. Thermotectonic evolution of the North Singhbhum Mobile Belt (Eastern India): A view from the western part of the belt. *Precambrian Research* 162, 102-127.
- Mazumder R., Van Loon A.J., Mallik L., Reddy S.M., Arima M., Altermann W., Eriksson P.G., De S., 2012. Mesoarchaeo-Palaeoproterozoic stratigraphic record of the Singhbhum Crustal Province, Eastern India: a synthesis. *Geological Society of London Special Publications* 365, 31-49.
- Meert J.G., 2002. Paleomagnetic evidence for a Paleo-Mesoproterozoic supercontinent Columbia. *Gondwana Research* 5, 207-215.
- Middlemost E.A.K., 1994. Naming materials in the magma/igneous system. *Earth Science Reviews* 37, 215-224.
- Montel J.M., Foret S., Veschambre M., Nicollet C., Provost A., 1996. Electron microprobe dating of monazite. *Chemical Geology* 131, 37-53.
- Mukherjee D. and Ghose N.C., 1992. Precambrian anorthosites within the Chhotanagpur Gneissic Complex. *Indian Journal of Geology* 64, 143-150.
- Mukhopadhyay D., 1990. Precambrian plate tectonics in the Eastern Indian Shield. In: *Crustal Evolution and Metallogeny*. (Eds.): S.P.H. Sychanthavong, Oxford and IBH Publishing Co, New Delhi, 75-100.
- Naganjaneyulu K. and Santosh M., 2010. The Central India Tectonic Zone: A geophysical perspective on continental amalgamation along a Mesoproterozoic suture. *Gondwana Research* 18, 547-564.
- Naha K. and Ghosh S.K., 1960. Archaean palaeogeography of E and N Singhbhum. *Geological Magazine* 97, 436-439.
- Pearce J.A., 2014. Immobile element fingerprinting of ophiolites. *Elements* 10, 101-108.
- Peccerillo A. and Taylor S.R., 1976. Geochemistry of Eocene calc-alkaline volcanic rocks from the Kastamonu area, northern Turkey. *Contributions to Mineralogy and Petrology* 58, 63-81.
- Pesonen L.J., Mertanen S., Veikkolainen T., 2012. Paleo-Mesoproterozoic supercontinents - a paleomagnetic view. *Geophysica* 48, 5-47.
- Pisarevsky S.A., Biswal T.K., Wang X.C., Waele B.D., Ernst R., Soderlund U., Tait J.A., Ratre K., Singh Y.K., Cleve M., 2013. Palaeomagnetic, geochronological and geochemical study of Mesoproterozoic Lakhna Dykes in the Bastar Craton, India: implications for the Mesoproterozoic supercontinent. *Lithos* 174, 125-143.
- Pradhan V.R., Meert J.G., Pandit M.K., Kamenov G., Gregory L.C., Malone S.J., 2009. India's changing place in global Proterozoic reconstructions: a review of geochronologic constraints and Paleomagnetic poles from the Dharwar, Bundelkhand and Marwar Cratons. *Journal of Geodynamics* 50, 224-242.
- Purohit K.K., Mukherjee P.K., Saini N.K., Khanna P.P., Rath M.S., 2006. Geochemical survey of stream sediments from upper parts of Alaknanda, Mandakini, Bhilangana and Bhagirathi Catchments, Garhwal Himalaya. *Himalayan Geology* 27, 31-39.
- Reddy S.M., Clarke C., Mazumder R., 2009. Temporal

- constraints on the evolution of the Singhbhum Crustal Province from U-Pb SHRIMP data. In: *Paleoproterozoic Supercontinents and Global Evolution*. (Eds.): D. Saha and R. Mazumder, International Association for Gondwana Research Conference Series 9, 17-18.
- Rekha S., Upadhyay D., Bhattacharya A., Kooijman E., Goon S., Mahato S., Pant N.C., 2011. Lithostructural and chronological constraints for tectonic restoration of Proterozoic accretion in the Eastern Indian Precambrian shield. *Precambrian Research* 187, 313-333.
- Rogers J.J.W. and Santosh M., 2002. Configuration of Columbia, a Mesoproterozoic supercontinent. *Gondwana Research* 5, 5-22.
- Roy A. and Prasad H., 2003. Tectonothermal events in Central Indian Tectonic Zone (CITZ) and its implications in Rodinian crustal assembly. *Journal of Asian Earth Sciences* 22, 115-129.
- Roy A., Kagami H., Yoshida M., Roy A., Bandyopadhyay B.K., Chattopadhyay A., Khan A.S., Huin A.K., Pal T., 2006. Rb-Sr and Sm-Nd dating of different metamorphic events from the Sausar Mobile Belt, central India: Implications for Proterozoic crustal evolution. *Journal of Asian Earth Sciences* 26, 61-76.
- Saikia A., Gogoi B., Ahmad M., Kumar R., Kaulina T., Bayanova T., 2019. Mineral Chemistry, Sr-Nd Isotope Geochemistry and Petrogenesis of the Granites of Bathani Volcano-Sedimentary Sequence from the Northern Fringe of Chotanagpur Granite Gneiss Complex of Eastern India. In: *Geological Evolution of the Precambrian Indian Shield*. (Eds.): M.E.A. Mondal, Society of Earth Scientists Series, Springer, Cham, 79-120.
- Saikia A., Gogoi B., Ahmad M., Ahmad T., 2014. Geochemical constraints on the evolution of mafic and felsic rocks in the Bathani volcano-sedimentary sequence of Chotanagpur Granite Gneiss Complex. *Journal of Earth System Science* 123, 959-987.
- Saikia A., Gogoi B., Kaulina T., Lialina L., Bayanova T., Ahmad M., 2017. Geochemical and U-Pb zircon age characterization of granites of Bathani volcano sedimentary sequence, Chotanagpur granite gneiss complex, eastern India: vestiges of Nuna supercontinent in central Indian tectonic zone. *Geological Society of London Special Publications* 457, 233-252.
- Saini N.K., Mukherjee P.K., Khanna P.P., Purohit K.K., 2007. A proposed amphibolite reference rock sample (AM-H) from Himachal Pradesh. *Journal of the Geological Society of India* 69, 799-802.
- Saini N.K., Mukherjee P.K., Rathi M.S., Khanna P.P., 2000. Evaluation of energy-dispersive x-ray fluorescence spectrometry in the rapid analysis of silicate rocks using pressed powder pellets. *X-ray Spectrometry* 29, 166-172.
- Saini N.K., Mukherjee P.K., Rathi M.S., Khanna P.P., Purohit K.K., 1998. A new geochemical reference sample of granite (DG-H) from Dalhousie, Himachal Himalaya. *Journal of the Geological Society of India* 52, 603-606.
- Sanyal S. and Sengupta P., 2012. Metamorphic evolution of the Chotanagpur Granite Gneiss Complex of the East Indian Shield: current status. *Geological Society of London Special Publications* 365, 117-145.
- Sarkar A.N., 1982. Precambrian tectonic evolution of eastern India: A model of converging microplates. *Tectonophysics* 86, 363-397.
- Sarkar S.N. and Saha A.K., 1977. The present status of the Precambrian stratigraphy, tectonics and geochronology of Singhbhum-Keonjhar-Mayurbhanj region, eastern India. *Indian Journal of Earth Sciences*, S. Ray Volume, 37-66.
- Sun S.S. and McDonough W.F., 1989. Chemical and isotopic systematics of oceanic basalts: Implications for mantle composition and processes. In: *Magmatism in ocean basins*. (Eds.): A.D. Saunders and M.J. Norry, Geological Society of London Special Publications 42, 313-345.
- Thieblemont D. and Cabanis B., 1990. Utilisation d'un diagramme (Rb/100)-Tb-Tapour la discrimination géochimique et l'étude pétrogénétique des roches magmatiques acides. *Bulletin de la Société Géologique de France* 6, 23-35.
- Wang Q., Hawkesworth C.J., Wyman D., Chung S.L., Wu F.Y., Li X.H., Li Z.X., Gou G.N., Zhang X.Z., Tang G.J., Dan W., Ma L., Dong Y.H., 2016. Pliocene-Quaternary crustal melting in central and northern Tibet and insights into crustal flow. *Nature Communications* 7, 11888.
- Woodhead J., Eggins S., Gamble J., 1993. High-field strength and transition element systematics in island arc and back-arc basin basalts: evidence for multiphase melt extraction and a depleted mantle wedge. *Earth and Planetary Science Letters* 114, 491-504.
- Yedekar D.B., Jain S.C., Nair K.K.K., Dutta K.K., 1990. The Central Indian collision suture. *Precambrian of Central India*. Geological Survey of India Special Publications 28, 1-37.
- Zhang S., Li Z.X., Evans D.A.D., Wu H., Li H., Dong J., 2012. Pre-Rodinia supercontinent Nuna shaping up: a global synthesis with new paleomagnetic results from North China. *Earth and Planetary Science Letters* 353-354, 145-155.
- Zhao G., Cawood P.A., Wilde S.A., Sun M., 2002. Review of global 2.1-1.8 Ga orogens: implications for a pre-Rodinia supercontinent. *Earth Science Reviews* 59, 125-162.



This work is licensed under a Creative Commons Attribution 4.0 International License CC BY. To view a copy of this license, visit <http://creativecommons.org/licenses/by/4.0/>